PNAS RESEARCH ARTICLE | ENGINEERING

Membrane stretch as the mechanism of activation of PIEZO1 ion channels in chondrocytes

Alireza Savadipour[a,b,c,d], Robert J. Nims[a,b,d], Neda Rashidi[a,b,c,d], Jaquelin M. Garcia-Castorena[a,b,d,e], Ruhang Tang[a,b,d], Gabrielle K. Marushack[a,b,d], Sara J. Oswald[a,b,d], Wolfgang B. Liedtke[f,g], and Farshid Guilak[a,b,c,d,e,h,1]

Edited by Kristi Anseth, University of Colorado Boulder, Boulder, CO; received December 28, 2022; accepted June 7, 2023

Osteoarthritis is a chronic disease that can be initiated by altered joint loading or injury of the cartilage. The mechanically sensitive PIEZO ion channels have been shown to transduce injurious levels of biomechanical strain in articular chondrocytes and mediate cell death. However, the mechanisms of channel gating in response to high cellular deformation and the strain thresholds for activating PIEZO channels remain unclear. We coupled studies of single-cell compression using atomic force microscopy (AFM) with finite element modeling (FEM) to identify the biophysical mechanisms of PIEZO-mediated calcium (Ca^{2+}) signaling in chondrocytes. We showed that PIEZO1 and PIEZO2 are needed for initiating Ca^{2+} signaling at moderately high levels of cellular deformation, but at the highest strains, PIEZO1 functions independently of PIEZO2. Biophysical factors that increase apparent chondrocyte membrane tension, including hypoosmotic prestrain, high compression magnitudes, and low deformation rates, also increased PIEZO1-driven Ca^{2+} signaling. Combined AFM/FEM studies showed that 50% of chondrocytes exhibit Ca^{2+} signaling at 80 to 85% nominal cell compression, corresponding to a threshold of apparent membrane finite principal strain of E = 1.31, which represents a membrane stretch ratio (λ) of 1.9. Both intracellular and extracellular Ca^{2+} are necessary for the PIEZO1-mediated Ca^{2+} signaling response to compression. Our results suggest that PIEZO1-induced signaling drives chondrocyte mechanical injury due to high membrane tension, and this threshold can be altered by factors that influence membrane prestress, such as cartilage hypoosmolarity, secondary to proteoglycan loss. These findings suggest that modulating PIEZO1 activation or downstream signaling may offer avenues for the prevention or treatment of osteoarthritis.

mechanobiology | mechanosensitive ion channel | mechanotransduction | osteoarthritis | cartilage

Altered joint loading or joint injury increases the risk of developing post-traumatic osteoarthritis (PTOA). While the mechanisms linking injury and PTOA are not fully understood, several studies have suggested that alterations in chondrocyte physiology or even cell death due to supraphysiologic strains may be in part responsible for the initiation and progression of joint degeneration (1). The PIEZO family of ion channels, consisting of PIEZO1 and PIEZO2, are expressed by cartilage-resident chondrocytes and respond to supraphysiologic levels of chondrocyte deformation (2). We previously found PIEZO inhibition reduced chondrocyte death during cartilage injury, suggesting the potential of these channels as therapeutic targets for PTOA (2, 3). While recent studies suggest that PIEZO activation is regulated by cellular membrane tension, it is unclear how whole-cell deformation relates to localized membrane tension as a potential mechanism for initiating PIEZO signaling (4, 5). Therefore, our goal was to determine the thresholds of mechanical strain that initiate cellular signaling by quantifying the physical signals that link cellular compression and PIEZO activation, in the context of chondrocyte responses to pathologic loading.

The biomechanical state of a cell, and its response to exogenous loading, is complex and depends upon interactions between the cell and the extracellular environment, including external forces, cytoskeletal proteins, cell-matrix interactions, and pericellular osmolarity, as well as intracellular conditions, including active cellular force generation, cellular stiffness, and viscoelasticity (6–22). The interface between these extracellular and intracellular conditions is the plasma membrane, where mechanosensitive ion channels, including the PIEZOs, directly respond to physical factors such as membrane stretch. Interestingly, while PIEZO activation has been attributed to increased tension in the plasma membrane, many cells, including chondrocytes, possess considerable membrane reservoirs, which endow a high degree of apparent extensibility that would occur prior to an actual stretch of the membrane bilayer (23). It is likely that membrane reservoirs would alter how externally applied forces contribute to and induce PIEZO signaling (24). However, because of the fine structure and properties of the plasma membrane, real-time optical measurements of membrane "stretch" per se are not possible with current microscopy techniques, and thus theoretical modeling

Significance

Post-traumatic osteoarthritis (PTOA) can develop following cartilage injury or altered loading and can result in progressive joint degeneration. A more detailed understanding of chondrocyte signaling in response to injury could provide new insights into the development of treatments for PTOA. We use single-cell mechanical stimulation to investigate the mechanisms by which PIEZO channels initiate chondrocyte Ca^{2+} signaling in response to injurious loading. PIEZO1 responds to supraphysiologic levels of chondrocyte deformation via increases in the cellular membrane tension to drive Ca^{2+} signaling. PIEZO1 signaling is modulated by different factors such as microenvironment osmolarity, loading magnitude and rate, and intracellular and extracellular Ca^{2+}. Our results suggest that modulation of PIEZO1 may provide a target for preventing chondrocyte death and osteoarthritis progression.

Competing interest statement: F.G. is a employee and shareholder of Cytex Therapeutics Inc. W.L. is an executive employee and shareholder of Regeneron Pharmaceuticals Inc.

This article is a PNAS Direct Submission.

[1]To whom correspondence may be addressed. Email: guilak@wustl.edu.

This article contains supporting information online at https://www.pnas.org/lookup/suppl/doi:10.1073/pnas.2221958120/-/DCSupplemental.

Published July 17, 2023.

approaches can provide critical insights into our understanding of membrane mechanics (25). Together, such a combined experimental and theoretical framework can improve our understanding of how cellular deformation modulates PIEZO mechanosensitivity.

Here, we investigated how mechanical compression induces PIEZO signaling and the implications of PIEZO signaling in cartilage injury. By coupling experimental atomic force microscopy (AFM) measurements with computational biomechanical models, we determined how bulk cellular compressive loading induces plasma membrane stretch to induce PIEZO activation. We further identified the specific roles of the osmotic environment, the magnitudes of applied force, and the rate of applied loading modulate PIEZO1 activation and observed that PIEZO1 activation requires both intracellular and extracellular Ca^{2+} sources. Together, our findings demonstrate how PIEZO1 is activated by membrane strain and is linked to external events including applied cellular compression and extracellular factors. This understanding of the mechanisms by which chondrocytes respond to supraphysiologic loading will provide important insights into the development of pharmacologic therapies to treat mechanically induced diseases such as PTOA.

Results

The Cooperation of PIEZO1 and PIEZO2 Is Dependent on the Magnitude of Loading. To investigate the role of PIEZO channels in chondrocyte mechanotransduction, we assessed the expression and mechanical responsiveness of the PIEZO channel family members PIEZO1 and PIEZO2 in chondrocytes. Both PIEZO1 and PIEZO2 channels were highly expressed in primary porcine chondrocytes (Fig. 1*A*), as we had previously found (2). To determine cellular mechanosensitivity, we mechanically compressed isolated chondrocytes with a tipless cantilever to 500 nN at a loading rate of 1 μm/s using atomic force microscopy (AFM) while monitoring the intracellular Ca^{2+} signaling response (2). To determine the roles of PIEZO1 and PIEZO2 in this process, we used small interfering RNA (siRNA) to knock down *PIEZO1* or *PIEZO2* gene expression before measuring the intracellular Ca^{2+} signaling response of the chondrocytes to a high applied mechanical load of 500 nN. qRT-PCR and western blotting confirmed the knockdown of PIEZO1 and PIEZO2 compared to the cells treated with a nontargeting control (NTC) siRNA. mRNA expression was reduced 87% for *PIEZO1* ($P < 0.0001$) and 72 to 76% for *PIEZO2* ($P < 0.0001$) while protein expression was reduced 67% for PIEZO1 and 61% for PIEZO2 compared to the NTC groups (Fig. 1 *B* and *C* and *SI Appendix*, Fig. S1*A*). AFM compression of 500 nN (Fig. 1 *D* and *F*) and 5 μM of Yoda1 (specific PIEZO1 agonist) pharmacologic stimulation (Fig. 1 *E* and *G*) induced robust Ca^{2+} signals in the NTC-treated chondrocytes. However, *PIEZO1* knockdown decreased Ca^{2+} signaling (AFM, $P < 0.0005$; Confocal, $P < 0.0001$) and the population of responsive cells to AFM compression or Yoda1 addition (AFM, $P < 0.05$; Confocal, $P < 0.0001$) (Fig. 1 *D* and *E* and Movies S1–S8). The

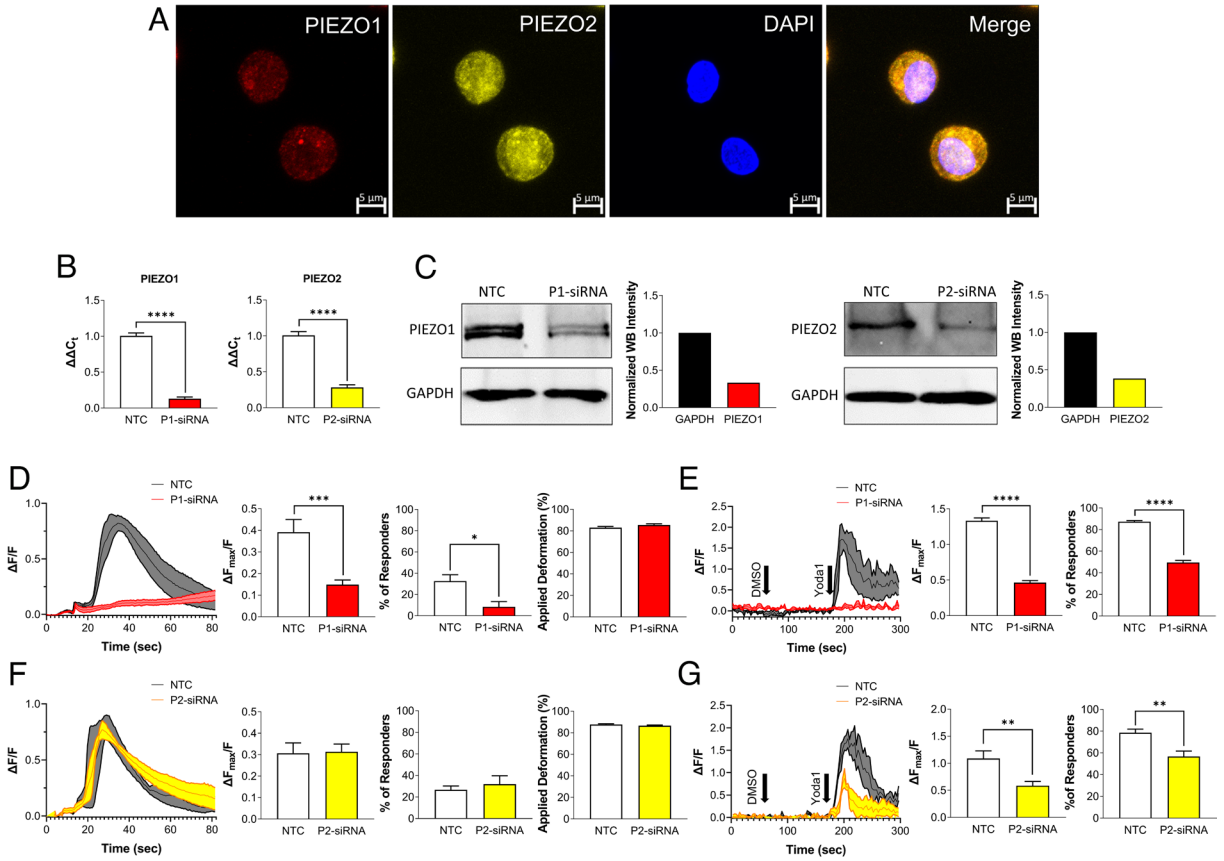

Fig. 1. Role of PIEZO1 and PIEZO2 in primary porcine chondrocytes during mechanical or pharmacologic activation. (*A*) Immunohistochemistry staining for PIEZO1 (red), PIEZO2 (yellow), and DAPI (blue). (Scale bar: 5 μm.) (*B*) mRNA levels of *PIEZO1* (P1) and *PIEZO2* (P2) normalized to ACTB expression level in nontargeting control (NTC) and P1-siRNA or P2-siRNA. (*C*) Protein levels of PIEZO1 (*Left*) and PIEZO2 (*Right*) in NTC and P1-siRNA or P2-siRNA chondrocytes. (*D*) AFM loading response of P1-siRNA cells compared to their respective NTCs showing representative cell signaling trend, normalized intracellular Ca^{2+} fluorescence intensity $\Delta F_{max}/F$, the percentage of the responding cells, and deformation. (*E*) Confocal imaging results of Yoda1 stimulation of P1-siRNA cells compared to their respective NTCs showing representative cell signaling trend, normalized intracellular Ca^{2+} fluorescence intensity $\Delta F_{max}/F$, and the percentage of responding cells. Similarly, results for P2-siRNA cells (*F*) AFM loading and (*G*) confocal imaging. Data presented as mean ± SEM. For *B*, n = 8 samples; for *D* and *F*, percentage of responders, n = 4 to 5 test batches, for applied deformation and Ca^{2+} response to AFM mechanical loading, n = 73 to 96 cells; For *E* and *G*, n = 9 to 21 tested wells; for group comparison *B*, *D*–*G*, *t* test, $*P < 0.05$, $**P < 0.005$, $***P < 0.001$, $****P < 0.0001$.

same experiments were performed on cells in which *PIEZO2* was knocked down using siRNA. Additionally, at loading magnitude of 100 nN, no cellular Ca^{2+} responses were observed in the NTC or P2-siRNA groups (*SI Appendix*, Fig. S1, $P = 0.8398$ for Ca^{2+} response, $P = 0.8524$ for percentage of the responding cells). At 300 nN force, P2-siRNA decreased chondrocyte Ca^{2+} response compared to NTC treated cells (*SI Appendix*, Fig. S1, $P < 0.005$ for Ca^{2+} response, $P < 0.05$ for percentage of the responding cells). At 500 nN AFM compression, however, the Ca^{2+} response and percentage of the responding cells were similar between *PIEZO2* knockdown and NTC-treated cells (Fig. 1*F*, $P = 0.906$ for Ca^{2+} response, $P = 0.572$ for percentage of the responding cells, Movies S1–S4). These findings indicate the presence of a cooperative mechanism between PIEZO1 and PIEZO2 that is strain magnitude dependent (2). Furthermore, *PIEZO2* knockdown significantly decreased the cellular response to the PIEZO1 agonist Yoda1 (Fig. 1*G*, $P = 0.0046$ for Ca^{2+} response, $P = 0.0037$ for percentage of the responding cells, Movies S5–S8). Previous studies have shown that the response to Yoda1 is reduced in cells with *PIEZO2* knockdown (26, 27). Importantly, we further compared the levels of applied deformation and found there were no significant differences between the NTC and P1-siRNA or P2-siRNA groups, demonstrating that the Ca^{2+} signaling changes to AFM compression were due to *PIEZO1* or *PIEZO2* knockdown and not alterations in the chondrocyte mechanical properties (Fig. 1 *D* and *F*, for P1-siRNA $P = 0.134$, and for P2-siRNA $P = 0.193$, *SI Appendix*, Fig. S1 *B* and *C*, $P = 0.6647$ for 300 nN, and $P = 0.5541$ for 100 nN). These results demonstrated that PIEZO1 and PIEZO2 interact and moderate levels of pathologic strain, but PIEZO1 serves as the primary mechanosensor at high, supraphysiologic mechanical loading, in this case 500 nN. As PIEZO1 was primarily responsible for conferring chondrocyte mechanosensitivity to high mechanical loads, we next sought to determine the relationship between the whole-cell compression and apparent membrane strain as a potential mechanism for the activation of PIEZO1.

PIEZO1 Mechanotransduction in Chondrocytes Is Modulated by Membrane Tension. While previous studies have suggested that PIEZO1 activation is regulated by cellular membrane tension (5, 28–30), chondrocytes possess highly ruffled membranes, complicating the relationship between cellular deformation, membrane tension, and ion channel activation (16, 23, 29, 31). Additionally, during daily activities, chondrocytes experience osmolarity changes within the range of 350 to 450 mOsm in healthy cartilage in the presence of all matrix components (32, 33). We hypothesized that modes of cellular loading which increase the cell membrane tension would elevate PIEZO1 activation. To test this hypothesis, we pretreated chondrocytes with solutions of various osmolarities to induce a cellular prestrain before performing AFM compressive loading and monitoring PIEZO1 activation via Ca^{2+} imaging. Chondrocytes are osmotically active cells and the application of isoosmotic (400 mOsm), hypoosmotic (200 mOsm), or hyperosmotic (600 mOsm) solutions were used to modulate the cellular membrane prestrain. After 2 h of osmotic prestimulation, compressive loads of 50 nN, 100 nN, 300 nN, or 500 nN were applied at the rate of 1 μm/s to test the chondrocytes' mechanosensitivity. Chondrocytes swelled under hypoosmotic treatment, crenated under hyperosmotic treatment (Fig. 2*A*, $P < 0.0001$), and were increasingly deformed at higher loads (Fig. 2*B*; Osmolarity, $P < 0.0001$; Force, $P < 0.0001$; Interaction, not significant). Intracellular Ca^{2+} signaling response was also increased at higher loads (Fig. 2 *C* and *D*; osmolarity, $P < 0.0001$; force, $P < 0.0001$; interaction, not significant, Movies S9–S12) resulting in an increase in the percentage of the cells which responded (Fig. 2*E*; Osmolarity, $P < 0.05$; Force, $P < 0.05$; Interaction, not significant). Interestingly, while cell deformation under hyperosmotic pretreatment was generally less than isoosmotic pretreatment, isoosmotic and hypoosmotic pretreated chondrocytes had similar deformations (Fig. 2*B*; Osmolarity, $P < 0.0001$; Force, $P < 0.0001$; Interaction, not significant). Despite the similar deformation levels between isoosmotic and hypoosmotic pretreatments, we found Ca^{2+} signaling was highest with isoosmotic pretreatment, particularly under 100 or 300 nN.

To investigate the relationship between osmolarity, membrane state, and membrane mechanosensitivity, we tested the hypothesis that the changes in apparent membrane strain were responsible for differences in compression-induced PIEZO1 activation and subsequent Ca^{2+} signaling among the different osmotic pretreatments. To estimate the apparent membrane strain under these different conditions, we performed finite element modeling (FEM) of the chondrocytes under AFM compression using FEBio software (http://www.febio.org/) (34). We fit the elastic modulus to the AFM deformation and force measurements of each cell and extracted the FEM-predicted maximal apparent membrane strain to assess how membrane tension varied under the different mechanical loading conditions. We found that the chondrocyte elastic moduli were similar under isoosmotic and hypoosmotic pretreatment but were significantly increased for cells under hyperosmotic pretreatment (Fig. 2*F*; osmolarity, $P < 0.0001$; force, $P < 0.0001$; interaction, $P < 0.0001$). Surprisingly, the models predicted the apparent membrane strain to be the highest under isoosmotic pretreatment in all loading groups compared to hypoosmotic and hyperosmotic pretreatment in all loading groups (Fig. 2*G*; osmolarity, $P < 0.0001$; force, $P < 0.0001$; interaction, $P < 0.05$). These results suggested cells in the isoosmotic condition experienced the highest level of membrane stretch independent of the loading magnitudes tested here. Moreover, when we plotted cellular response to the FEM-predicted apparent membrane strain, we found cells in the isoosmotic condition have the highest number of responding cells and level of membrane strain in all loading configurations (Fig. 2*H*). Since the isoosmotic treatment groups had the most prominent Ca^{2+} response and highest levels of deformation when loaded to 50, 100, 300, and 500 nN, we used these conditions to determine the apparent membrane strain using FEM. For this group, we plotted the signaling intensity and fraction of responsive cells against the level of compression to determine the compression levels necessary to induce strong Ca^{2+} signaling and at least 50% responsive cells (Fig. 2 *I*–*K*). These data show that the mean Ca^{2+} response began increasing above nominal cellular deformations of 65% (Fig. 2*I*), and a deformation range of ~80 to 85% (indicated by * in Fig. 2*J*) was necessary to induce signaling in 50% of compressed chondrocytes. The 80 to 85% range of cellular compression was shown to result in a range of apparent membrane strains (maximum principal strain E) of 1.31 to 1.90, which shows a tensile membrane stretch ratio (λ) of 1.9 to 2.19. This result indicates that stretching the membrane to 190 to 219% of the original dimensions (i.e., a 90 to 119% increase) represents the threshold of apparent membrane stretch that induces intracellular Ca^{2+} response in 50% of the cells (Fig. 2*K*). Interestingly, our FE model suggests that cellular compression of 65 to 75% corresponds to the high end of the toe region for the apparent membrane strain curve. In this region, a small change in deformation does not significantly affect the slope of the curve. Specifically, the FE model predicts an apparent membrane strain between 0.56 and 0.98 at the high end of the toe region. The two highest forces we tested, 300 nN and 500 nN, correspond to points where the apparent membrane strain rapidly steepens past

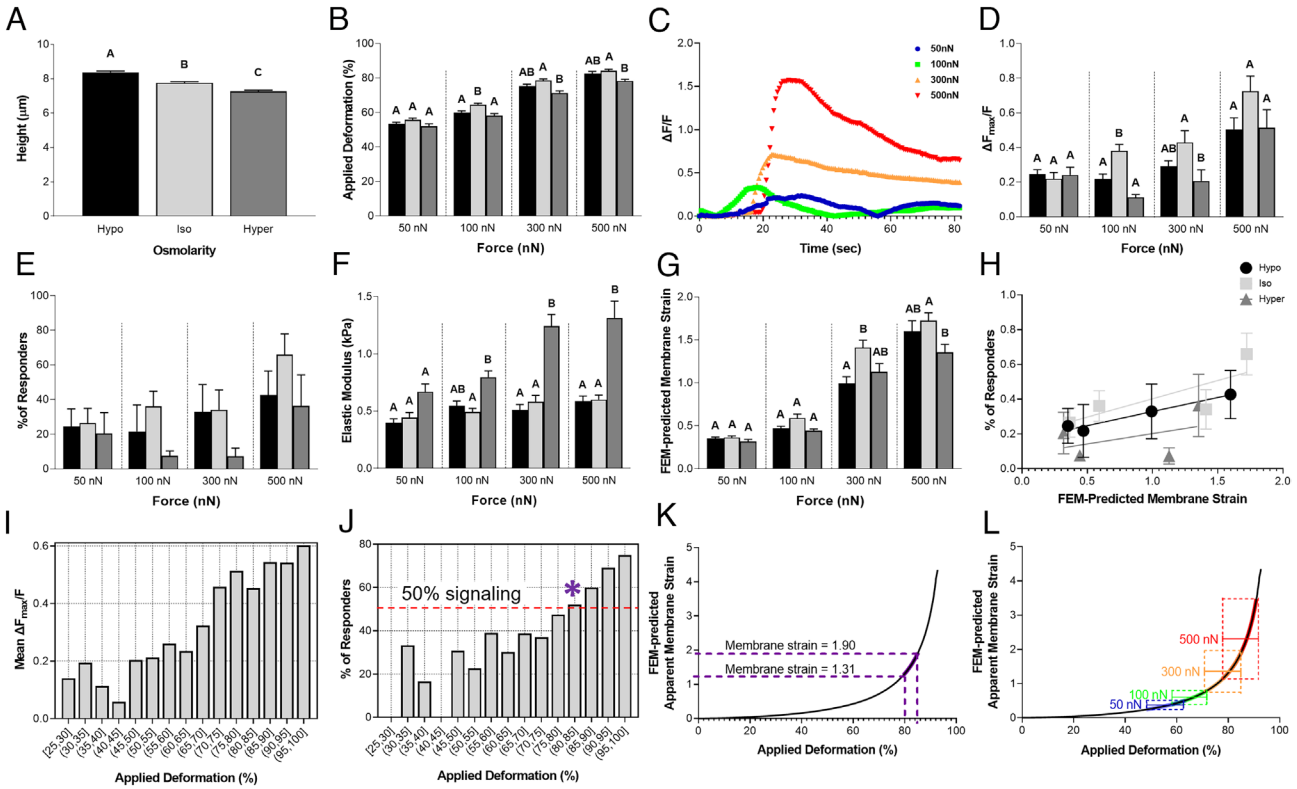

Fig. 2. Chondrocyte intracellular Ca^{2+} response to AFM mechanical loading after long-term (2 h) osmotic conditions, with finite element modeling (FEM) to estimate membrane strain response. (*A*) Chondrocyte height measured by AFM for long-term osmotic conditions: hypoosmotic (200 mOsm), isoosmotic (400 mOsm) and hyperosmotic (600 mOsm). (*B*) Applied deformation (%) at different forces for each osmotic condition. (*C*) Trend of signaling in the representative cells in isoosmotic condition. (*D*) AFM loading response of chondrocytes showing normalized intracellular Ca^{2+} fluorescence intensity $\Delta F_{max}/F$ for each osmotic condition. (*E*) Percentage of the responding cells to different AFM loading conditions. (*F*) Elastic modulus (kPa) of chondrocytes calculated with FEM in each loading condition. (*G*) FEM-predicted apparent membrane strain levels in each loading condition. (*H*) Relation between the percentage of the responding cells and the FEM-predicted apparent membrane strain in different osmotic conditions. (*I*) The level of mean Ca^{2+} intensity in different deformation ranges. (*J*) The frequency of Ca^{2+} response in different deformation ranges. The * indicates the deformation range by which greater than 50% of the cells responded to the mechanical loading. (*K*) Aligned 80 to 85% applied deformation range to FEM-predicted apparent membrane strain against applied deformation curve in isoosmotic condition to determine the apparent membrane strain levels within this deformation range. (*L*) FEM-predicted apparent membrane strain plotted against applied deformation in isoosmotic condition with overlayed applied deformation (%) while loading the chondrocytes to 50, 100, 300, and 500 nN. Data presented as mean ± SEM. For group comparison A, one-way ANOVA with Tukey's post hoc test, different letters indicate statistical significance, $P < 0.05$, n = 219 to 266 cells; For group comparison *B*, *D*–*G*, one-way ANOVA with Tukey's post hoc test within the groups with the same loading magnitude, different letters indicate statistical significance $P < 0.05$; For *B*, *D*–*G*, to find the effect of osmolarity, loading magnitude, and their interactions, two-way ANOVA with Tukey's post hoc test was performed; n = 46 to 67 cells for *B*, *D*, *F*, and *G* and n = 4 to 5 test batches for *E*.

the toe region, and experimentally, they resulted in the highest levels of cellular Ca^{2+} signaling.

Using FEM, we then determined the range of magnitudes of apparent cell membrane stretch in response to increasing levels of mechanical compression. To do so, we overlayed the average level of applied deformation that we obtained by loading the chondrocytes to 50, 100, 300, and 500 nN ± 1 SD of the mean (SD) to the FEM curve [FEM-predicted apparent membrane strain against applied deformation (%)] (Fig. 2*L*). In this manner, we were able to determine the range of apparent membrane strain that cells underwent while being compressed to different levels. Our FEM findings predict that increasing the loading magnitude and the resulting higher levels of cellular deformation drastically increased the apparent membrane strain applied to the cell, in a nonlinear manner (Fig. 2*L*).

Short-Term Hypoosmotic Pretreatment Increased PIEZO1 Mechanosensitivity. We next sought to investigate whether the signaling response following osmotic pretreatment was time dependent, potentially being modulated by the cellular volume regulatory response to maintain homeostasis (23, 35–39). To investigate the short-term and long-term effects of osmotic changes on cellular volume regulation, we assessed the mechanosensitivity of chondrocytes to hypoosmotic or isoosmotic conditions by pretreating them with hypoosmotic or isoosmotic solutions for either 30 s (short-term) or 2 h (long-term) prior to mechanical compression. AFM loading to 500 nN was performed at a compression rate of 1 μm/s. Cell height was significantly increased after hypoosmotic pretreatment, with cells pretreated for 30 s having a higher cell height than cells pretreated for 2 h (Fig. 3*A*; osmolarity, $P < 0.005$; treatment duration, $P < 0.0001$; interaction, not significant). There was no significant difference in cell deformation between the chondrocytes pretreated with hypoosmotic and isoosmotic solutions for 2 h (Fig. 3*B*; $P = 0.9810$). However, there was a significant reduction in the applied deformation of the cells pretreated with hypoosmotic solution for 30 s compared to the isoosmotic group (Fig. 3*B*; $P < 0.0001$). There was a significant increase in Ca^{2+} signaling with 30 s of hypoosmotic pretreatment compared to the isoosmotic and long-term hypoosmotic-treated groups (Fig. 3 *C* and *D*; osmolarity, $P < 0.0001$; treatment duration, $P < 0.0001$; interaction, $P < 0.0001$). Additionally, a higher percentage of chondrocytes responded to mechanical loading after 30 s of hypoosmotic pretreatment (62%) compared to those pretreated with isoosmotic solution (43%) (Fig. 3*E*). To determine the chondrocytes' membrane tension due to loading and the hypoosmotic stress, we again used FEM to examine the chondrocyte mechanical state 30 s after pretreatment. Our FEM analysis showed

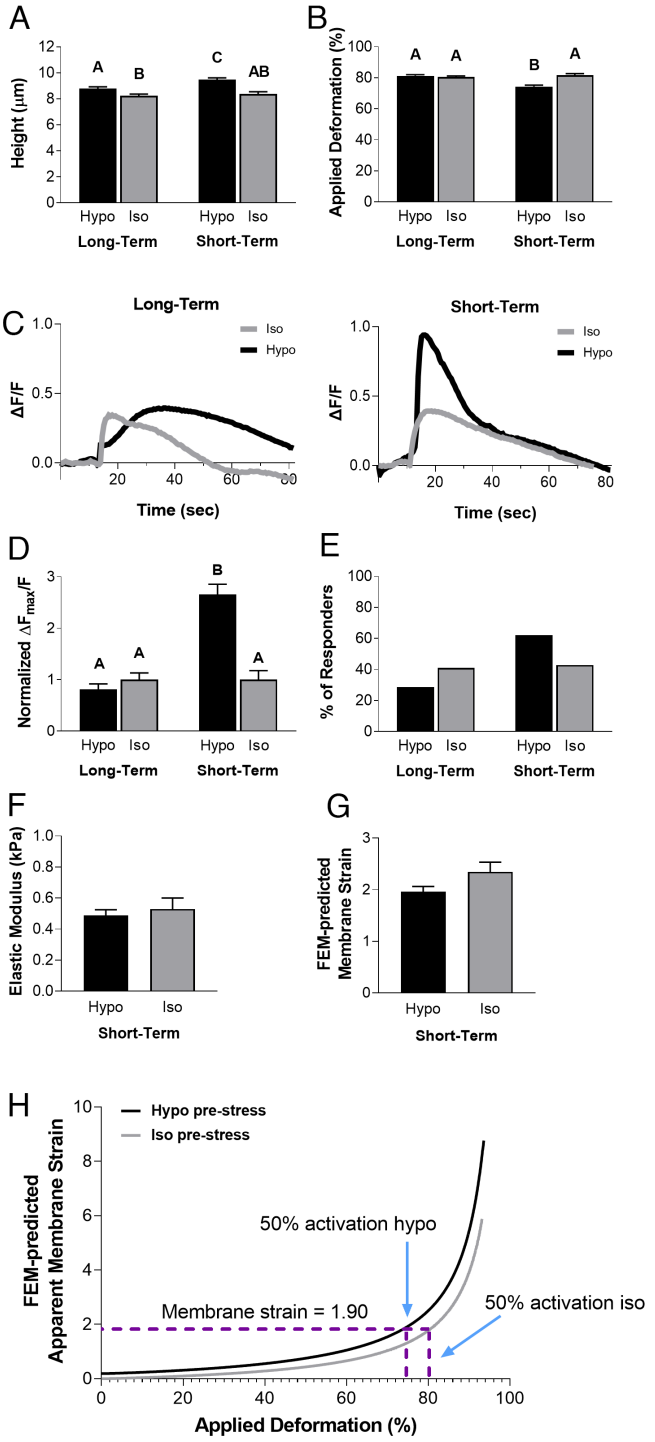

Fig. 3. Chondrocyte intracellular Ca^{2+} response to AFM mechanical loading at 500 nN comparing long-term (2 h) hypoosmotic exposure and short-term (30 s) hypoosmotic challenge, with FEM to estimate membrane strain levels. (*A*) Chondrocyte heights in long-term (2 h) and short-term (30 s) exposure to hypoosmotic (200 mOsm) and iso osmotic (400 mOsm) conditions, as measured by AFM. (*B*) Applied deformation (%) for all conditions. (*C*) Trend of intracellular Ca^{2+} response for all conditions in representative cells. (*D*) Intracellular Ca^{2+} fluorescence intensity $\Delta F_{max}/F$ normalized to isoosmotic condition values. (*E*) Percentage of responding cells for each condition. (*F*) Elastic modulus (kPa) calculated with FEM. (*G*) Apparent membrane strain levels calculated with FEM. (*H*) FEM-predicted apparent membrane strain plotted against applied deformation (%) curves for isoosmotic and hypoosmotic challenges. Data presented as mean ± SEM. For group comparison *A*, *B*, and *D*, two-way ANOVA with Tukey's post hoc test, different letters indicate statistical significance $P < 0.05$, n = 35 to 58 cells; For group comparison *F* and *G*, *t* test, n = 35 to 58 cells, no significance found.

that the elastic moduli of chondrocytes were similar between isoosmotic and hypoosmotic pretreatment (Fig. 3*F*; $P = 0.5836$). Additionally, there were no significant differences in the predicted apparent membrane strain levels between the two groups (Fig. 3*G*; $P = 0.0516$). Interestingly, when we ran a model simulation to include a hypoosmotic challenge prior to AFM compression, the apparent membrane strain level was consistently higher, despite the same level of deformation in the cells (Fig. 3*H*). For instance, more than 80% deformation in the isoosmotic condition was required to reach the 1.31 maximum principal membrane strain E (which corresponds to a stretch ratio of $\lambda = 1.9$) that induces intracellular Ca^{2+} response in 50% of the chondrocytes, however, less than 75% deformation is necessary to reach the same level of apparent membrane strain in the hypoosmotic-treated cells. This suggests that hypoosmotic stress can elevate the apparent membrane strain prior to loading. In conclusion, our experimental results indicate that membrane prestrain due to hypoosmotic stress could increase the mechanosensitivity of chondrocytes and PIEZO1 activation. However, extended periods of pretreatment were associated with volume recovery and reduced this hypoosmotic sensitivity. Our FEM analysis showed that increases in cellular membrane strain during compression of hypoosmotic pretreated cells may sensitize PIEZO1 activation, while the recovery of cellular size back to isoosmotic control levels after 2 h may act to minimize the osmotically induced membrane prestrain. These findings suggest that changes in cellular volume regulation play a critical role in modulating chondrocyte mechanosensitivity and provide important insights into the regulation of mechanotransduction in chondrocytes.

Chondrocyte Viscoelasticity Governs PIEZO1 Activation and Downstream Ca^{2+} Signaling. Our observations indicated that PIEZO1 activation was time- and membrane state-dependent and show that PIEZO1 activation is influenced by cellular viscoelasticity. To assess the influence of cellular viscoelastic properties on PIEZO1 mechanosensitivity, we applied 500 nN of compression at rates of 1 μm/s, 5 μm/s, 10 μm/s, or 15 μm/s under isoosmotic conditions. Consistent with a viscoelastic material, chondrocytes experienced different levels of deformation when loaded at different rates. As the loading rate increased, the cellular deformation levels decreased significantly (Fig. 4*A*; $P < 0.0001$), as so did the Ca^{2+} response (Fig. 4 *B* and *C*; $P = 0.0095$), and the percentage of cells exhibiting a Ca^{2+} response (Fig. 4*D*; $P = 0.0015$). Therefore, these results indicate that mechanosensation via PIEZO1 activation is influenced by cellular viscoelasticity due to differences in the magnitude of cellular deformation, with increased cellular deformations resulting in increased intracellular Ca^{2+} responses. However, when only the Ca^{2+} response of responding cells was analyzed, there was no significant effect of loading rate (Fig. 4*E*; $P = 0.3272$).

While we found that Ca^{2+} signaling was dependent on the rate of loading, we were surprised to find that responsive cells exhibited similar levels of Ca^{2+} response (Fig. 4*E*; $P = 0.3272$). We hypothesized that the relationship between Ca^{2+} response and viscoelasticity was driven by PIEZO1 activation and then subsequently amplified by downstream pathways. To identify the mechanosensitive origins of the loading rate sensitivity, we treated chondrocytes with varying inhibitors to either block the sources of intracellular and extracellular Ca^{2+} signaling or inhibit PIEZO1 activity before applying different rates of compressive loading. PIEZO1 was blocked using the non-specific inhibitor GsMTx-4, intracellular Ca^{2+} release was blocked using thapsagargin, and extracellular Ca^{2+} influx was blocked using ethylene glycol-bis(β-aminoethyl ether)-N,N,N′,N′-tetraacetic acid

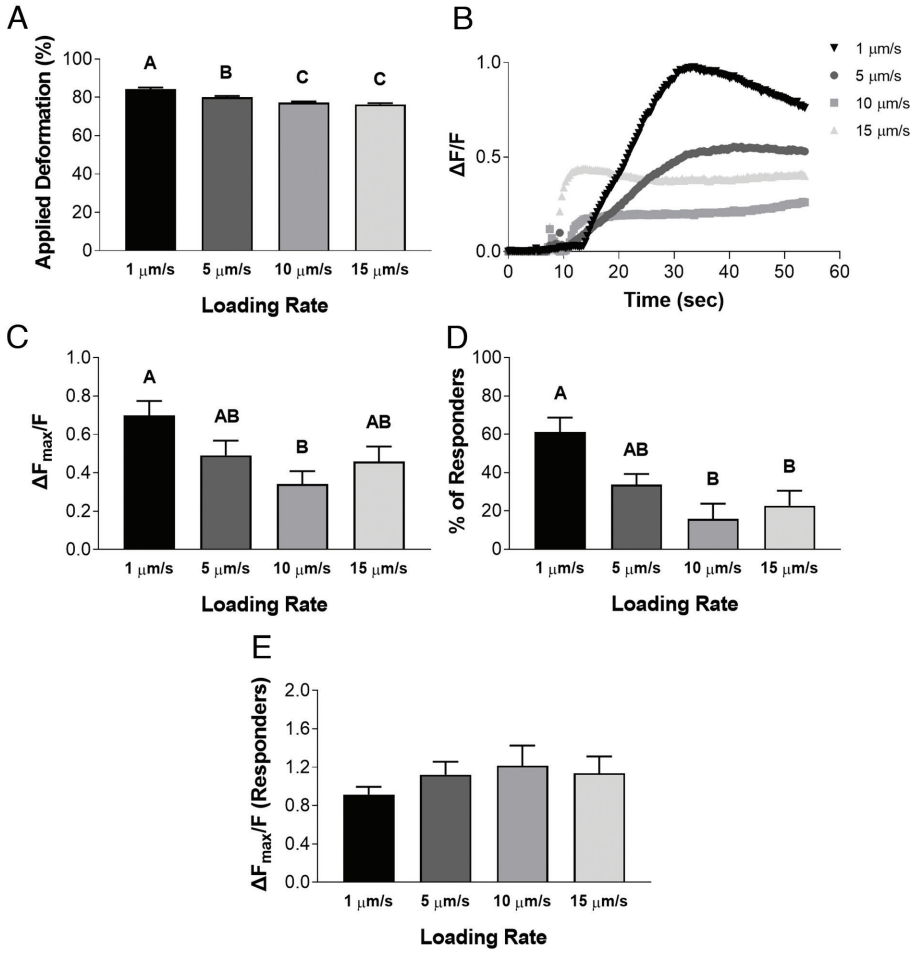

Fig. 4. Chondrocyte Ca^{2+} response to AFM mechanical loading at different loading rates. (*A*) Applied deformation (%) measured for each loading rate. (*B*) Representative signaling trend for each loading rate. (*C*) Intracellular Ca^{2+} fluorescence intensity $\Delta F_{max}/F$ for each loading rate. (*D*) Percentage of responding cells for each loading rate. (*E*) Considering only the responding cells, intracellular Ca^{2+} fluorescence intensity $\Delta F_{max}/F$ for each loading rate. Data presented as mean ± SEM. For group comparison *A*, *C*, *D*, and *E*, one-way ANOVA with Tukey's post hoc test, different letters indicate statistical significance $P < 0.05$ with no significance found in *E*, n = 51 to 61 cells.

(EGTA) (Fig. 5 *A*–*C*). Notably, the inhibitors did not alter the mechanical properties of the cells, as no significant changes in cellular deformation levels were observed in response to the mechanical compression within the groups (Fig. 5*A*; $P = 0.1330$–0.2051). At all rates, GsMTx-4, thapsigargin, and EGTA attenuated the intracellular Ca^{2+} response and the percentage of the responding cells (Fig. 5 *B* and *C*; $P < 0.0001$ for 1, 5, and 10 μm/s; $P = 0.0002$ for 15 μm/s). Interestingly, when loaded at a rate of 1 μm/s, which induces the most Ca^{2+} signaling, the non-specific PIEZO1 inhibitor GsMTx-4 significantly reduced the Ca^{2+} response while still maintaining a similar fraction of responsive cells compared to the control (Fig. 5*C*). Our results also indicate that PIEZO1 activation is sensitive to cellular viscoelasticity as mediated by the magnitude of overall deformation, and therefore, the subsequent increase in membrane strain. Furthermore, these data show that both intracellular and extracellular sources of Ca^{2+} are necessary to amplify the Ca^{2+} signaling initiated by PIEZO1 activation.

Discussion

Our findings indicate that PIEZO activation in response to chondrocyte deformation depends on the magnitude of the apparent membrane strain that occurs as the cell is compressed and deforms (expands) laterally (Fig. 6). Specifically, we identified that supraphysiologic cellular compression leads to tensile stretch of the membrane that activates PIEZO1, and factors that influence membrane stretch can therefore modulate Ca^{2+} in response to compression. Decreasing extracellular osmolarity, increasing loading magnitude, and lowering loading rate sensitize PIEZO1 activity through increases in the apparent membrane strain, ultimately leading to increases in mechanically induced Ca^{2+} signaling. Mechanically sensitive ion channels have been hypothesized to be activated by either strain or stress stimuli (40). Our data support the notion that cellular deformation (i.e., strain) leads to bulging of the cell at its "equator," leading to unfolding of the extracellular plasma membrane and tensile membrane stretch that drives PIEZO1 activation. Therefore, on a cellular basis, PIEZO1 activation is driven by distortions within the plasma membrane and flattening of the membrane curvatures. More specifically, the unique shape of the PIEZO1 channel which includes multiple transmembrane domains, presence of specific amino acids within the channel, and large extracellular domain, allows PIEZO1 to be a mechanosensor for cell stretch (41, 42). We further found that the extracellular and intracellular sources of Ca^{2+} are necessary for PIEZO1 activity but are insensitive to the rate of loading, suggesting PIEZO1 is the critical sensor of cellular deformation and thus, dependent on the viscoelastic properties of the cell.

Previous studies have suggested that PIEZO channels are activated through increased apparent membrane tension. However, the relationship between whole-cell deformation and

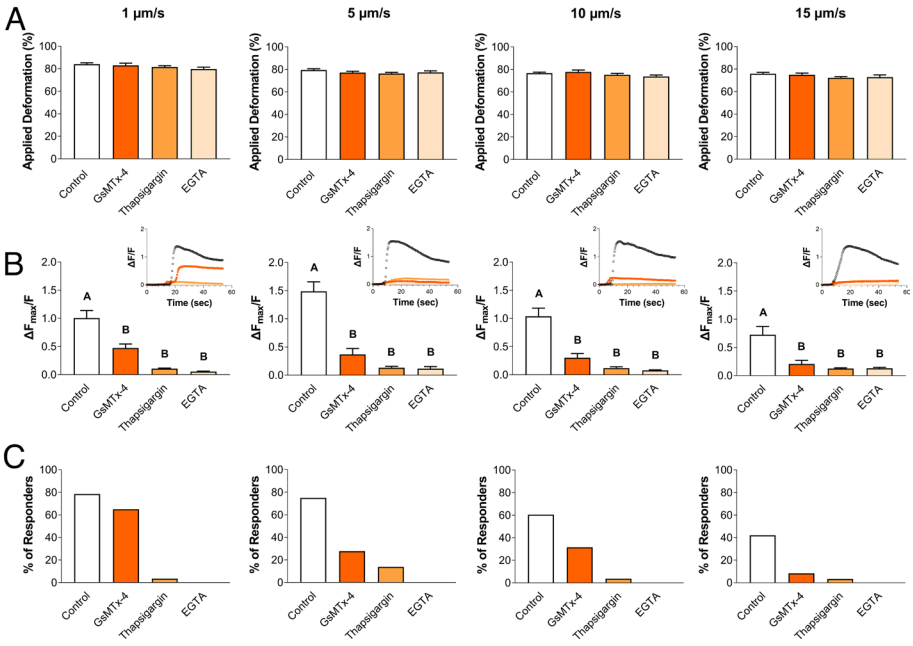

Fig. 5. Ca^{2+} signaling of chondrocytes in response to different mechanical loading rates in the presence of PIEZO1 nonspecific inhibitor GsMTx-4 and Ca^{2+} inhibitors thapsigargin and EGTA. (*A*) Applied deformation (%). (*B*) Intracellular Ca^{2+} fluorescence intensity $\Delta F_{max}/F$, with *Inset* showing representative signaling trends. (*C*) Percentage of responding cells. Data presented as mean ± SEM. For group comparison *A* and *B*, one-way ANOVA with Tukey's post hoc test, different letters indicate statistical significance $P < 0.05$ with no significance found in *A*, n = 12 to 42 cells.

thresholds of membrane tension required to achieve PIEZO1 activation is complex (5, 16, 29). By combining our AFM and Ca^{2+} signaling experimental data with FEM of the whole chondrocyte's deformation, we specifically determined that an apparent membrane strain threshold of 1.31 is required for 50% probability of cellular response to mechanical compression through the PIEZO1 channel. This value suggests that large cellular deformations are required to activate the PIEZO1

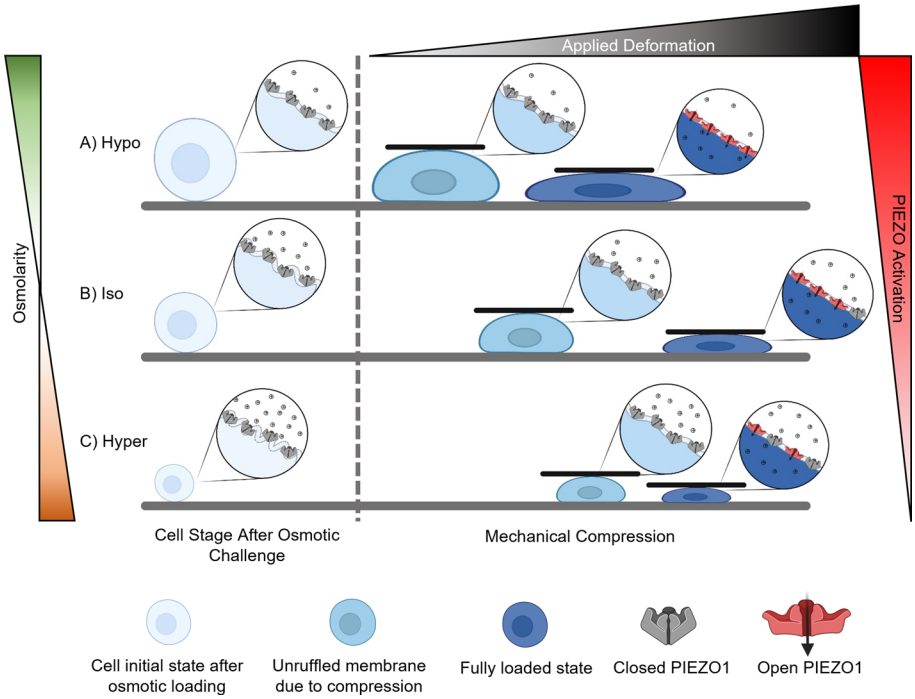

Fig. 6. Schematic of the mechanism involved in PIEZO1 activation in response to membrane tension. As the cell is deformed and experiences tensile strains in the peripheral regions, the cell plasma membrane initially experiences unfolding. After the ruffles are unfolded, then the plasma membrane will experience local tensile strains. However, swelling of the cell with (*A*) hypoosmotic stress unfolds the ruffles prior to loading and exposes more PIEZO channels to the extracellular cues before mechanical compression, resulting in higher levels of intracellular Ca^{2+} signaling in the chondrocytes in response to mechanical compression compared to the (*B*) isoosmotically treated group. (*C*) On the other hand, applying a hyperosmotic stress decreases the cell size and increases membrane ruffling. Therefore, more deformation is required to unfold the membrane curvatures before inducing stretch of the plasma membrane. Consequently, the force and deformation necessary to unfold the membrane curvatures increase compared to the isoosmotically treated group. This change results in a smaller portion of the force being dedicated to compressing the cell and decreases the sensitivity of the PIEZO channel to mechanical compression.

channel and induce subsequent Ca^{2+} signaling in chondrocytes with high membrane ruffling. Although this threshold is considerably higher than the 2 to 4% area extension (43) that a phospholipid membrane can withstand, our findings are consistent with the presence of significant ruffled membrane reservoirs in chondrocytes (44). The reservoirs enable the chondrocyte membrane to withstand this high level of apparent membrane strain without rupturing under normal physiologic levels of cartilage compression.

Furthermore, we found that increasing the loading magnitude significantly enhances the intracellular Ca^{2+} response of the chondrocytes under direct mechanical compression. This conclusion is consistent with previous findings that suggest higher magnitudes of load can unruffle more areas of the membrane (31). Consequently, this phenomenon would expose more mechanosensitive channels to the external cues, increase membrane tension to higher levels, and increase the cellular Ca^{2+} response (2). Previous studies have also shown that under hypoosmotic loading, similar to levels imposed in our study, the surface area of the chondrocyte membrane can expand to 234% of the membrane surface area present under isoosmotic conditions before the membrane ruptures, which supports our findings here (23).

Our results further described a biphasic modulation of membrane tension during cell swelling and cell crenation in activating PIEZO1. Cell crenation under hyperosmotic stimulation and cell swelling under hypoosmotic stimulation reduced PIEZO1 activation compared to isoosmotic stimulation when allowed to equilibrate to the pretreatment (i.e., the long-term treatment regimen). Interestingly, short-term hypoosmotic pretreatment was necessary to induce increased PIEZO1 activation through cellular swelling, suggesting a prominent role of chondrocyte active remodeling to modulate mechanosensitivity (36, 45–48). These results demonstrate that only transient membrane prestrain enhanced PIEZO1 response to compressive loading and that over longer durations, chondrocytes remodel and attenuate their PIEZO1 mechanosensitivity. Our FEM analysis predicted a slightly increased apparent membrane strain under isoosmotic conditions compared to hypoosmotic conditions owing to an increase in cellular deformation in the isoosmotic group. As our mechanical models do not consider the active cellular remodeling under osmotic stresses, the actual apparent membrane strain is likely to be altered as the cell remodels to achieve homeostasis. Conversely, by applying a short-term hypoosmotic stress that partially unruffles the membrane, we found that the sensitization of PIEZO1 to mechanical compression significantly increased compared to the isoosmotic-treated group. Together, these results suggest that transiently increasing the membrane tension increases PIEZO1 activation and chondrocyte mechanoresponse. Understanding how chondrocytes modify their mechanosensitivity in response to loading will provide valuable insights for developing refined FE models of chondrocyte mechanosensation. Furthermore, cross talk between PIEZO1 and other chondrocyte mechanosensors may be a crucial aspect for understanding chondrocyte function under physiological and supraphysiologic loading conditions. Of note, our findings confirm and extend our previous observation of potential synergy between PIEZO1 and PIEZO2 in chondrocyte mechanosensing (2). Consistent with previous findings, we found that Ca^{2+} signaling due to moderately high levels of cell deformation (at 300 nN) were reduced by either P1-siRNA or P2-siRNA, suggesting that PIEZO1 and PIEZO2 cooperate at these levels of membrane stretch (2). However, at the highest levels of loading (500 nN), P2-siRNA had no inhibitory effect, and PIEZO1 appears to function independently at this point. This important finding suggests that the synergy between PIEZO1 and PIEZO2 is dependent on the magnitude of membrane stretch.

Furthermore, we show initial evidence of PIEZO1–PIEZO2 interaction with chemical activation, as P2-siRNA reduced the Ca^{2+} response to Yoda1 (Fig. 1 *E* and *G*). Because Yoda1 is a highly specific activator of PIEZO1, this finding supports the notion that PIEZO1 activation be modulated by the presence of PIEZO2 in the membrane. This finding is consistent with several previous studies that show similar trends in other cell types (26, 27). While the mechanisms underlying these interactions remain to be determined, these findings paint a complex and expanding picture of chondrocyte mechanobiology and its underlying "channelome" (3, 49).

While osmotic loading in chondrocytes can also induce the activation of other ion channels, including transient receptor potential vanilloid-4 (TRPV4), the dynamics of activation observed in this study suggest that the response to direct loading is predominantly driven by PIEZO1. We previously demonstrated that blocking TRPV4 did not alter chondrocyte mechanosensitivity to direct compression by AFM loading (50). Moreover, Ca^{2+} fluctuations by PIEZO1 are distinct from other mechanosensitive ion channels, characterized by different inactivation times (28, 51–55). Consequently, the downstream targets induced by PIEZO1 activation are known to differ from those induced by other mechanosensitive ion channels. Moreover, Lee et al. showed that blocking PIEZO channels using their nonspecific inhibitor GsMTx-4 prior to applying a hypoosmotic stress increased the Ca^{2+} response and the responsive cell fraction to a hypoosmotic challenge (2), indicating a possible interaction of the PIEZO channels with TRPV4 in chondrocytes to regulate mechanosensitive currents. Additionally, we found that high cellular deformations and membrane strains are specific to PIEZO1 activation and not sufficient to trigger PIEZO2 activation. Interestingly, applying 300 nN force to the P2-siRNA chondrocytes, which would induce a cellular deformation similar to our previous study (2), decreased the level of intracellular Ca^{2+} response in the cells, showing that the synergy between PIEZO1 and PIEZO2 exists up to a certain level of deformation. However, PIEZO1 is the only channel that responds above a certain level of mechanical deformation. Furthermore, we observed evidence of PIEZO1/PIEZO2 interaction in the response to Yoda1, consistent with previous studies on different cell types that have suggested potential reduction in PIEZO1 activation with *PIEZO2* knockdown (26, 27). These findings support the notion of synergy between PIEZO1 and PIEZO2 and suggest that these interactions are dependent on the magnitude of deformation as well as the mode channel of activation.

Our results, showing that either chelating extracellular Ca^{2+} or inhibiting the release of intracellular Ca^{2+} blocks the whole-cell PIEZO1-induced Ca^{2+} response, support the mechanism of Ca^{2+}-induced Ca^{2+} release downstream to PIEZO1 activation. These findings suggest that mechanical stretch initially induces a Ca^{2+} flux through the membrane, which results in greater Ca^{2+} release from intracellular storages. However, it is possible that other channels may further regulate the gating of PIEZO1 or other Ca^{2+} sources. Future studies may wish to investigate the roles of the synergy between mechanosensitive ion channels and other types of channels, such as voltage-gated Ca^{2+} permeable ion channels (VGCCs). Previous studies have suggested that the activation of a mechanosensitive channel can induce the activation of VGCCs by polarizing the membrane (56). These studies may identify targets for treating PIEZO1-related pathologies.

Our findings are consistent with previous studies suggesting that cellular level mechanical strain is a primary mediator of chondrocyte death at high loads (57, 58). Furthermore, these findings provide mechanistic insight on previous reports that have shown chondroprotective effects of medium solutions with increased

osmolarity (59), suggesting that altering the sequence of mechanically induced Ca^{2+} signaling may have an influence on chondrocyte viability, and potentially, cartilage health. Additional work is needed to determine the downstream targets involved in mechanically mediated chondrocyte death, which may include inflammatory mediators such as NF-κB (60), nitric oxide (61), and subsequent mitochondrial dysfunction (62, 63). Furthermore, inflammatory mediators such as interleukin 1 may in turn alter the activity of mechanosensitive channels such as PIEZO1 or TRPV4 (64–66), potentially providing a positive feedback loop to exacerbate pathologic responses in chondrocytes.

Our study also revealed that the chondrocytes' mechanical properties, specifically its viscoelasticity, can influence PIEZO1 mechanosensation. To block PIEZO1 activity in these loading conditions, we used GsMTx-4, a nonspecific PIEZO inhibitor (67–71). Results indicated that application of GsMTx-4 significantly decreased the response of chondrocytes to mechanical loading in all loading conditions. Moreover, the cellular Ca^{2+} response and percentage of the responders were also rate dependent even with the application of GsMTx4. The fact that GsMTx4-treated cells respond at low loading rates suggests that PIEZO1 is the primary responder to the rate of cellular deformation. Further, the finding that inhibiting extracellular Ca^{2+} sources diminished the PIEZO1 response to mechanical compression is consistent with our previous study (2). Our finding, that PIEZO1 activity is driven by the rate of loading, opens a perspective on how cells may use feedback control between their mechanosensors and their mechanics to maintain homeostasis. Additionally, previous studies have shown that viscoelastic effects of the extracellular environment can be sensed by TRPV4 (72, 73). Therefore, understanding the feedback between cell mechanics, extracellular mechanics, and these cell mechanosensors will be an important area of future research for understanding mechanically driven disease pathogenesis. Additionally, investigating the possible variation in mechanosensitivity of the PIEZO1 channel in chondrocytes from different zones or regions in the cartilage is another important question that needs to be answered in future studies.

In summary, we found that PIEZO1 activation is driven during chondrocyte deformation by the concomitant increases in membrane tension through depleting intracellular Ca^{2+} reservoirs. Using FE models, we determined that an apparent membrane strain of 1.31 is the approximate threshold of strain, which is necessary for the PIEZO1 activation with the probability of 50%. Our investigation of the different factors which play essential roles in amplifying PIEZO1 Ca^{2+}signaling demonstrated that extracellular conditions, including the osmolarity, Ca^{2+} sources, loading rate, and magnitude, differentially drive PIEZO1 Ca^{2+}signaling. Future characterization of these downstream effects may offer a promising therapeutic opportunity for treating cartilage injuries. Together, our findings deconstruct the initial activation and downstream coordination of PIEZO1 signaling and establish mechanical thresholds and therapeutic entry points for treating PTOA.

Materials and Methods

Cell Culture and Sample Preparation. The knees of skeletally mature pigs (5 to 6 mo old, mixed breeds of landrace yorkshire and duroc) were acquired on the day of slaughter from a local abattoir shop. The articular cartilage of the femoral midcondyle was cut out and maintained in standard culture media [High glucose Dulbecco's Modified Eagle Medium (DMEM, Gibco, Thermo Fisher Scientific), 10% fetal bovine serum (FBS, Atlas Biologicals), 1.5% HEPES (Corning), 1% MEM Nonessential amino acid (Corning), 1% Pen Strep (Gibco, Thermo Fisher Scientific), 0.5% L-Proline (Sigma Aldrich)] for 1 to 2 d prior to digestion. The tissue was digested in pronase (Worthington Biochemical) dissolved in the wash media [High glucose DMEM, 1× Gentamycin (Gibco, Thermo Fisher Scientific), 1× Kanamycin (Goldbio), 1× Fungizone (Corning)] (1,320 PKU/mL media) for 1 to 1.5 h. Next, the pronase-containing media were removed from the tissue, and the tissue was incubated for 3 to 3.5 h with media containing 0.4% collagenase type II (Worthington Biochemical). Last, the cells were filtered, washed, resuspended in the growth media (10% FBS, 1.5% HEPES, 2% Pen/Strep), counted and plated on 12-mm round coverslips #1.5 (Electron Microscopy Sciences) with the concentration of 50,000 to 100,000 cells/coverslip for the AFM study. For the confocal studies, the cells were plated in high-resolution glass-bottom 96-well plates (Cellvis). The cells were cultured for 3 d in an incubator (5% CO_2, 37 °C) prior to testing. The wash and growth medium osmolarity was kept at 380 to 400 mOsm to mitigate the physiological conditions in cartilage (32, 33).

Atomic Force Microscopy. Primary chondrocytes were compressed using an atomic force microscope (AFM; MFP-3D Bio, Asylum Research). Prior to testing, the cells were labeled with Fura2-AM dye (Invitrogen, Thermo Fisher Scientific), an intracellular Ca^{2+}-sensitive dye, in media (Phenol red free DMEM, Gibco, Thermo Fisher Scientific), with 1.5% HEPES buffer (Corning), 1% Pen Strep (Gibco Thermo Fisher Scientific), 1% MEM nonessential amino acid (Corning), 1% Na Pyruvate (Corning), 1% GlutaMax (Gibco, Thermo Fisher Scientific), 0.1% L-Proline (Sigma Aldrich) for 1 to 2 h. Chondrocytes were compressed using a tipless cantilevers with approximate stiffness of 7 to 13 N/m (Nanoandmore). The stiffness of the cantilevers was measured using the thermal method provided by the manufacturer. While cells were being loaded, 340/380-nm wavelength light sources were used to capture ratiometric Ca^{2+} images. All the experiments were performed at 37 °C in a hydrated environment. Cells that moved during imaging or were damaged (as noted by rapid loss of intracellular fluorescence) were not included in the analysis. The obtained AFM curves, which show the amount of indentation against the vertical displacement of the cantilever, were analyzed using a custom written MATLAB code (The Math Works, Inc., https://www.mathworks.com) to find the contact point, cell height, and cellular deformation in response to loading. Moreover, the videos of cells' intracellular Ca^{2+} response to mechanical loading were analyzed using ImageJ software (U. S. NIH, Bethesda, MD, https://imagej.nih.gov/ij/).

Confocal Microscopy. Nucleofected cells were stained for 1 h prior to imaging using Fura red-AM (Invitrogen, Thermo Fisher Scientific) and Fluo4-AM (Invitrogen, Thermo Fisher Scientific), which are Ca^{2+} indicator dyes elucidating the changes in the level of Ca^{2+} concentration in the cell. After labeling, cells were washed and placed under a confocal microscope (LSM 880, Zeiss, Dublin, CA). The temperature during imaging was kept at 37 °C to keep the environment similar to physiological conditions. After 1 min of baseline imaging, control solution (dimethyl sulfoxide, Sigma Aldrich) was added to the cells, and the cells were imaged for another 2 min. After control imaging, final concentration of 5 μM of Yoda1 was added to the cells, and the cellular response was imaged for another 2 min. All labeling, washing, and imaging steps were performed in isoosmotic conditions. After imaging, the videos were analyzed in ImageJ to quantify the level of Ca^{2+} response of each cell during imaging.

Image Analysis. We analyzed the images from confocal and AFM experiments in ImageJ. Briefly, we exported the videos to ImageJ and divided the two channels that represent the fluo-4 and fura-red in the confocal imaging or 340-nm and 380-nm wavelength light sources that excited the fura-2 in the AFM experiment by each other to show the normalized intensity of the signal. Then, by thresholding the videos based on the staining intensity, we acquired and analyzed the shape of the cells in terms of pixel intensity throughout the whole experiment. Afterward, we normalized the mean pixel intensities to the baseline level of the signal. Finally, we reported the maximum value of normalized pixel intensity for each cell as the intracellular Ca^{2+} response of the cell ($\Delta F_{max}/F$).

To separate the responders and nonresponders in the AFM studies, we performed a control test in which the cantilever was located on top of the cells, but no load was applied. Afterward, we analyzed the Ca^{2+} transient within those cells, normalized it, and calculated the mean (M) and SD of the intracellular Ca^{2+} response of those cells. We considered any cellular Ca^{2+} response higher than the average of the control group plus three times the SD of the mean ($\Delta F_{max}/F > M + 3*SD$) that had a peak in its intracellular Ca^{2+} response trace as a responder. Therefore, any cell whose Ca^{2+} response was lower than that value or did not have a peak in its Ca^{2+} response trace was considered as a non-responder.

For the confocal experiment analysis, we analyzed the videos in ImageJ and reported the $\Delta F_{max}/F$ of each cell for each experiment. We then processed these

results using a custom-written MATLAB code to find the percentage of the responding cells and the average level of intracellular Ca^{2+} signaling. Using the MATLAB code, we normalized individual cell's intracellular Ca^{2+} response to Yoda1 addition to the cell's response after the control solution addition. Then, we determined the average of the $\Delta F_{max}/F$ of all the cells and reported it as the mean cellular response calculated from each video. Moreover, the MATLAB code evaluated whether the $\Delta F_{max}/F$ of a cell was higher than the average of the cellular Ca^{2+} signal after control solution addition ($M^{'}$) plus five times the SD of the mean ($SD^{'}$) ($\Delta F_{max}/F > M^{'} + 5*SD^{'}$). If so, we considered the cell as a responder. Finally, we reported the total number of the responders divided by the total number of the cells as the percentage of the responding cells for each video. If there were more than four values for the responding cells, meaning the experiment was performed on more than four different animals, we reported the individual values for the percentage of the responding cell. However, if we had less than four values per group, we reported the average of all the results and reported a single value for the percentage of the responding cells.

Osmotic Treatment. Osmolarity of the media was changed by adding sucrose (Sigma Aldrich) to make either the hyperosmotic (600 mOsm) or isosmotic (400 mOsm) solution, or by adding ultrapure 18 Megaohm water to achieve the hypoosmotic solution (200 mOsm). The media were then filtered and used for osmotic treatments.

siRNA. Chondrocytes were isolated as previously described and immediately nucleofected with siRNA targeting the porcine (Sus scofra) *PIEZO1* mRNA (a pool of siRNAs with the following sequence strands:

5′-CAGCGAGAUCUCGCACUCCAUCUU-3′, 5′-UACGACCUGCUGCAGCUCCUGUU-3′, and 5′-ACCCGCUGGCCAUGCAGUUCUUUU-3′ all synthesized from Dharmacon), *PIEZO2* mRNA (pool of siRNAs with the following sense strands:

5′-GAUCUGCGUGGAGGACAUUUAUGUU-3′, and

5′-CGACGAAGUCGAACAGUGAGUGUU-3′all synthesized from Dharmacon), or a nontargeting construct siRNA (siNTC, Invitrogen, Thermo Fisher Scientific). Nucleofection was performed using the Lonza (Basel, Switzerland) 4D-Nucleofector according to the manufacturer's guidelines, utilizing the ER-100 protocol. Nucleofected cells were plated on glass coverslips, 96-well plate, or six-well plates depending on the experiments, in FBS-containing feed media without Pen-strep. After 3 d of culture, cells were either collected for qRT-PCR or western blot analysis or stained for AFM or confocal imaging.

RNA Isolation and qRT-PCR. The cells were plated after nucleofection, and the mRNA was isolated after 3 d of culture (Norgen, Total RNA Purification Plus kit, Thorold, ON, Canada) and quantified using a NanoDrop. Afterward, the cDNA was synthesized from mRNA (VILO Superscript Mastermix, Life Technologies) and real-time qPCR was run using the cDNA with fast SYBR Green Master mix (Thermo Fisher Scientific). The delta delta Ct ($\Delta\Delta$Ct) method was used to quantify the relative expression of the genes of interest, and finally the expression levels were normalized to the ACTB mRNA levels. The sequence of the primers used is listed below.

PIEZO1: Forward 5′-GCCCCCAACGGACCTGAAGC-3′
Reverse 3′-TGCGCAGCTGG ATACGCACC-5′
PIEZO2: Forward 5′-CCAGCTGGATCTGCGTGGAGG-3′
Reverse 3′-TGGTTGATCACC CCGGCGAC-5′
ACTB: Forward 5′-CACGCCATCCTGCGTCTGGA-3′
Reverse 3′-AGCACCGTGTTGG CGTAGAG-5′

Immunolabeling. After 3 d of culturing cells on round coverslips, media were washed, and cells were fixed with 4% paraformaldehyde (Electron Microscopy Sciences) for 10 min. Then, cells were washed with 2× Dulbecco's phosphate-buffered saline (DPBS, Gibco) followed by cell permeabilization with 0.3% Triton X-100 (Sigma) in DPBS for 5 min. Afterward, 2.5% normal goat serum (Vector Laboratories) was added for 45 min to block the cells. Last, samples were labeled with conjugated rabbit PIEZO1 and PIEZO2 antibodies overnight (1:25, Novus Biologicals). After immunolabeling, the cells were washed with DPBS and stored at 4 °C until imaging.

Western Blot. To examine the effect of siRNA knockdown on *PIEZO1* and *PIEZO2* expression in porcine chondrocytes at protein levels, western blot analysis was performed. Protein concentration was measured using the Pierce BCA Protein Assay (Thermo Fisher Scientific) after lysing in RIPA buffer (Cell Signaling Technology) with 2.5% CHAPS (Sigma Aldrich) and protease inhibitor (Thermo Fisher Scientific). Each well of a 6% sodium dodecyl sulfate-polyacrylamide electrophoresis gel was loaded with 25-μg protein or prestained molecular weight markers (Thermo Fisher Scientific). The transferred polyvinylidene fluoride (PVDF) membranes were incubated overnight at 4 °C with the primary antibodies: anti-PIEZO1 (1:1,000, Proteintech, #15939-1-AP), anti-PIEZO2 (1:300, Alomone labs, Jerusalem, Israel, #APC-090), anti-GAPDH (1:20,000, Proteintech #60004-1-Ig) for *PIEZO1* knockdown, *PIEZO2* knockdown, or loading control, respectively. Afterward, the membrane was incubated with HRP-conjugated secondary antibodies (1:3,000, Cell Signaling Technology). Immunoblots were imaged and analyzed using the iBright FL1000 Imaging System (Thermo Fisher Scientific). Normalized western blot intensity represents the signal intensity divided by the area of protein bands in arbitrary units after normalization to the signal intensity of GAPDH.

Chemical Inhibition of Ca^{2+} Signaling. Inhibitors were used to evaluate the effect of several factors on the mechanosensitivity of the PIEZO1 channel. We used GsMTx-4 to show that the responses to mechanical loading and different rates of loading are due to the activation of the PIEZO1 channel. We used EGTA and thapsigargin to determine the role of extracellular and intracellular Ca^{2+} sources, respectively, in the activation of the PIEZO1 channel. The concentration of each inhibitor and the duration of treatment are as follows: GsMTx-4 (20 μM, 15 min prior to loading, Alomone Lab), EGTA (10 mM, Sigma Aldrich), and Thapsigargin (3 μM, 30 min prior to loading, Sigma Aldrich).

Finite Element Modeling (FEBio). To assess the mechanical influence of different loading conditions, we developed a neo-Hookean FE model of the cell during AFM compression using FEBio software (v. 2.6, www.febio.org). The model was fitted to the force/deflection AFM curves to determine the elastic modulus. Moreover, the model consisted of a homogeneous cytoplasm phase and a shell element to represent the cell membrane, both of which were fit to the same neo-Hookean model. The cell was considered to be axisymmetric in shape and have axisymmetric boundary conditions. Therefore, we modeled 1/8 of the cell to find the elastic modulus under different osmotic and mechanical conditions. The cell was considered to be incompressible ($v = 0.4999$) and a Lagrangian contact point between the cell and the cantilever was developed to enhance the quality of the contact. The apparent membrane strain was acquired from the model using the principal Lagrangian strain (E) of the membrane shell material, and the membrane tensile stretch was calculated using the Green strain equation $\lambda = \sqrt{2E + 1}$, where λ is the stretch ratio and E is the principal strain. The strain in the undeformed cell model (prior to compression or osmotic effects) was assumed to be zero, i.e., a stretch ratio of 1. To model osmotic shock, we used a material mixture of Neo-Hooken and cell growth along with an additional step of loading before the mechanical compression to simulate the short-term hypoosmotic treatment.

Statistical Analysis. Average of the groups is presented in each plot with ±SEM. Statistical analysis was performed by student *t* test, one-way, or two-way ANOVA followed by Tukey post hoc to determine the significance between each group, $P < 0.05$.

Data, Materials, and Software Availability. All data needed to evaluate the conclusions in the paper are present in the paper. All study data are included in the article and/or supporting information.

ACKNOWLEDGMENTS. This work was supported by the Shriners Hospitals for Children, the NIH (AG15768, AG46927, AR080902, AR072999, AR073752, and AR074992), and NRSA fellowship F32 AR074240 to R.J.N.

Author affiliations: [a]Department of Orthopaedic Surgery, Washington University in St. Louis, St. Louis, MO 63110; [b]Shriners Hospitals for Children – St. Louis, St. Louis, MO 63110; [c]Department of Mechanical Engineering and Materials Science, Washington University in St. Louis, St. Louis, MO 63110; [d]Center of Regenerative Medicine, Washington University in St. Louis, St. Louis, MO 63110; [e]Division of Biology and Biomedical Sciences, Biochemistry, Biophysics, and Structural Biology Program, Washington University in St. Louis, St. Louis, MO 63110; [f]Department of Neurology, Duke University, Durham, NC 27705; [g]Department of Molecular Pathobiology, New York University College of Dentistry, New York, NY 10010; and [h]Department of Biomedical Engineering, Washington University in St. Louis, St. Louis, MO 63110

Author contributions: A.S., R.J.N., W.B.L., and F.G. designed research; A.S., R.J.N., N.R., R.T., and G.K.M. performed research; A.S., R.J.N., N.R., J.M.G.-C., R.T., G.K.M., S.J.O., and W.B.L. analyzed data; and A.S., R.J.N., J.M.G.-C., S.J.O., and F.G. wrote the paper.

1. I. Pountos, P. V. Giannoudis, Modulation of cartilage's response to injury: Can chondrocyte apoptosis be reversed? *Injury* **48**, 2657–2669 (2017).
2. W. Lee *et al.*, Synergy between Piezo1 and Piezo2 channels confers high-strain mechanosensitivity to articular cartilage. *Proc. Natl. Acad. Sci. U.S.A.* **111**, E5114–E5122 (2014).
3. W. Lee, F. Guilak, W. Liedtke, "Role of piezo channels in joint health and injury" in *Current Topics in Membranes* (Elsevier, 2017), pp. 263–273.
4. C. A. Haselwandter, R. MacKinnon, Piezo's membrane footprint and its contribution to mechanosensitivity. *Elife* **7**, e41968 (2018).
5. Y.-C. Lin *et al.*, Force-induced conformational changes in PIEZO1. *Nature* **573**, 230–234 (2019).
6. G. A. Ateshian, K. D. Costa, C. T. Hung, A theoretical analysis of water transport through chondrocytes. *Biomech. Model. Mechanobiol.* **6**, 91–101 (2007).
7. S.-K. Han *et al.*, In situ chondrocyte viscoelasticity. *J. Biomech.* **45**, 2450–2456 (2012).
8. W. R. Trickey, G. M. Lee, F. Guilak, Viscoelastic properties of chondrocytes from normal and osteoarthritic human cartilage. *J. Orthopaedic Res.* **18**, 891–898 (2000).
9. W. R. Trickey, T. P. Vail, F. Guilak, The role of the cytoskeleton in the viscoelastic properties of human articular chondrocytes. *J. Orthopaedic Res.* **22**, 131–139 (2004).
10. C. Van Donkelaar, W. Wilson, Mechanics of chondrocyte hypertrophy. *Biomech. Model. Mechanobiol.* **11**, 655–664 (2012).
11. S. V. Eleswarapu, N. D. Leipzig, K. A. Athanasiou, Gene expression of single articular chondrocytes. *Cell Tissue Res.* **327**, 43–54 (2007).
12. N. D. Leipzig, K. A. Athanasiou, Static compression of single chondrocytes catabolically modifies single-cell gene expression. *Biophys. J.* **94**, 2412–2422 (2008).
13. G. Ofek, D. C. Wiltz, K. A. Athanasiou, Contribution of the cytoskeleton to the compressive properties and recovery behavior of single cells. *Biophys. J.* **97**, 1873–1882 (2009).
14. A. Shieh, K. Athanasiou, Dynamic compression of single cells. *Osteoarthritis Cartilage* **15**, 328–334 (2007).
15. A. C. Shieh, K. A. Athanasiou, Principles of cell mechanics for cartilage tissue engineering. *Ann. Biomed. Eng.* **31**, 1–11 (2003).
16. C. D. Cox *et al.*, Removal of the mechanoprotective influence of the cytoskeleton reveals PIEZO1 is gated by bilayer tension. *Nat. Commun.* **7**, 1–13 (2016).
17. E. J. Koay, G. Ofek, K. A. Athanasiou, Effects of TGF-β1 and IGF-I on the compressibility, biomechanics, and strain-dependent recovery behavior of single chondrocytes. *J. Biomech.* **41**, 1044–1052 (2008).
18. E. J. Koay, A. C. Shieh, K. A. Athanasiou, Creep indentation of single cells. *J. Biomech. Eng.* **125**, 334–341 (2003).
19. J. K. Lee *et al.*, Tension stimulation drives tissue formation in scaffold-free systems. *Nat. Mater.* **16**, 864–873 (2017).
20. G. Ofek *et al.*, Biomechanics of single chondrocytes under direct shear. *Biomech. Model. Mechanobiol.* **9**, 153–162 (2010).
21. G. Ofek, R. M. Natoli, K. A. Athanasiou, In situ mechanical properties of the chondrocyte cytoplasm and nucleus. *J. Biomech.* **42**, 873–877 (2009).
22. A. C. Shieh, E. J. Koay, K. A. Athanasiou, Strain-dependent recovery behavior of single chondrocytes. *Biomech. Model. Mechanobiol.* **5**, 172 (2006).
23. F. Guilak, G. R. Erickson, H. P. Ting-Beall, The effects of osmotic stress on the viscoelastic and physical properties of articular chondrocytes. *Biophys. J.* **82**, 720–727 (2002).
24. J. L. Nourse, M. M. Pathak, "How cells channel their stress: Interplay between Piezo1 and the cytoskeleton" in *Seminars in Cell & Developmental Biology* (Elsevier, 2017).
25. E. P. Carpenter *et al.*, Overcoming the challenges of membrane protein crystallography. *Curr. Opin. Struct. Biol.* **18**, 581–586 (2008).
26. M. G. Dalghi *et al.*, Functional roles for PIEZO1 and PIEZO2 in urothelial mechanotransduction and lower urinary tract interoception. *JCI insight* **6**, e152984 (2021).
27. G. Parsonage *et al.*, Improved PIEZO1 agonism through 4-benzoic acid modification of Yoda1. *Br. J. Pharmacol.*, 10.1111/bph.15996 (2022).
28. D. J. Beech, A. C. Kalli, Force sensing by piezo channels in cardiovascular health and disease. *Arteriosclerosis Thrombosis Vascular Biol.* **39**, 2228–2239 (2019).
29. A. H. Lewis, J. Grandl, Mechanical sensitivity of Piezo1 ion channels can be tuned by cellular membrane tension. *Elife* **4**, e12088 (2015).
30. J. Wu, A. H. Lewis, J. Grandl, Touch, tension, and transduction–the function and regulation of Piezo ion channels. *Trends Biochem. Sci.* **42**, 57–71 (2017).
31. E. K. Moo, W. Herzog, Unfolding of membrane ruffles of in situ chondrocytes under compressive loads. *J. Orthopaedic Res.* **35**, 304–310 (2017).
32. T. Mang, S. Lindemann, A. Gigout, Increasing the medium osmolarity reduces the inflammatory status of human OA chondrocytes and increases their responsiveness to GDF-5. *Int. J. Mol. Sci.* **21**, 531 (2020).
33. S. Sieber *et al.*, Importance of osmolarity and oxygen tension for cartilage tissue engineering. *BioResearch Open Access* **9**, 106–115 (2020).
34. S. A. Maas *et al.*, FEBio: Finite elements for biomechanics. *J. Biomech. Eng.* **134**, 011005 (2012).
35. P. G. Bush, A. C. Hall, The osmotic sensitivity of isolated and in situ bovine articular chondrocytes. *J. Orthopaedic Res.* **19**, 768–778 (2001).
36. P. G. Bush, A. C. Hall, Regulatory volume decrease (RVD) by isolated and in situ bovine articular chondrocytes. *J. Cell. Physiol.* **187**, 304–314 (2001).
37. P. G. Bush, A. C. Hall, The volume and morphology of chondrocytes within non-degenerate and degenerate human articular cartilage. *Osteoarthritis Cartilage* **11**, 242–251 (2003).
38. P. G. Bush *et al.*, Viability and volume of in situ bovine articular chondrocytes–changes following a single impact and effects of medium osmolarity. *Osteoarthritis Cartilage* **13**, 54–65 (2005).
39. P. G. Bush, C. A. Parisinos, A. C. Hall, The osmotic sensitivity of rat growth plate chondrocytes in situ; clarifying the mechanisms of hypertrophy. *J. Cell. Physiol.* **214**, 621–629 (2008).
40. B. Martinac, Mechanosensitive ion channels: Molecules of mechanotransduction. *J. Cell Sci.* **117**, 2449–2460 (2004).
41. X.-Z. Fang *et al.*, Structure, kinetic properties and biological function of mechanosensitive Piezo channels. *Cell Biosci.* **11**, 1–20 (2021).
42. W. Li, N. Gao, M. Yang, The structural basis for sensing by the Piezo1 protein. *Curr. Top. Membranes* **79**, 135–158 (2017).
43. E. A. Evans, R. Waugh, L. Melnik, Elastic area compressibility modulus of red cell membrane. *Biophys. J.* **16**, 585–595 (1976).
44. E. K. Moo *et al.*, The properties of chondrocyte membrane reservoirs and their role in impact-induced cell death. *Biophys. J.* **105**, 1590–1600 (2013).
45. G. R. Erickson, L. G. Alexopoulos, F. Guilak, Hyper-osmotic stress induces volume change and calcium transients in chondrocytes by transmembrane, phospholipid, and G-protein pathways. *J. Biomechanics* **34**, 1527–1535 (2001).
46. R. Lewis, C. H. Feetham, R. Barrett-Jolley, Cell volume regulation in chondrocytes. *Cell. Physiol. Biochem.* **28**, 1111–1122 (2011).
47. M. N. Phan *et al.*, Functional characterization of TRPV4 as an osmotically sensitive ion channel in porcine articular chondrocytes. *Arthritis Rheumatism Off. J. Am. College Rheumatol.* **60**, 3028–3037 (2009).
48. Z. Wang *et al.*, The rate of hypo-osmotic challenge influences regulatory volume decrease (RVD) and mechanical properties of articular chondrocytes. *Osteoarthritis Cartilage* **23**, 289–299 (2015).
49. A. Mobasheri *et al.*, The chondrocyte channelome: A narrative review. *Joint Bone Spine* **86**, 29–35 (2019).
50. R. J. Nims *et al.*, A synthetic mechanogenetic gene circuit for autonomous drug delivery in engineered tissues. *Sci. Adv.* **7**, eabd9858 (2021).
51. P. A. Gottlieb, F. Sachs, Piezo1: Properties of a cation selective mechanical channel. *Channels* **6**, 214–219 (2012).
52. B. Nilius, J. Prenen, G. Owsianik, Irritating channels: The case of TRPA1. *J. Physiol.* **589**, 1543–1549 (2011).
53. B. Nilius *et al.*, TRPV4 calcium entry channel: A paradigm for gating diversity. *Am. J. Physiol. Cell Physiol.* **286**, C195–C205 (2004).
54. B. Nilius, H. Watanabe, J. Vriens, The TRPV4 channel: Structure-function relationship and promiscuous gating behaviour. *Pflügers Archiv.* **446**, 298–303 (2003).
55. R. Syeda *et al.*, Chemical activation of the mechanotransduction channel Piezo1. *elife* **4**, e07369 (2015).
56. M. Hara *et al.*, Calcium influx through a possible coupling of cation channels impacts skeletal muscle satellite cell activation in response to mechanical stretch. *Am. J. Physiol. Cell Physiol.* **302**, C1741–C1750 (2012).
57. P. F. Argote *et al.*, Chondrocyte viability is lost during high-rate impact loading by transfer of amplified strain, but not stress, to pericellular and cellular regions. *Osteoarthritis Cartilage* **27**, 1822–1830 (2019).
58. F. Guilak, A. Ratcliffe, V. C. Mow, Chondrocyte deformation and local tissue strain in articular cartilage: A confocal microscopy study. *J. Orthopaedic Res.* **13**, 410–421 (1995).
59. A. K. Amin *et al.*, Osmolarity influences chondrocyte death in wounded articular cartilage. *JBJS* **90**, 1531–1542 (2008).
60. I. M. Berke *et al.*, NF-κB-mediated effects on behavior and cartilage pathology in a non-invasive loading model of post-traumatic osteoarthritis. *Osteoarthritis Cartilage* **29**, 248–256 (2021).
61. D. E. Prince, J. K. Greisberg, Nitric oxide-associated chondrocyte apoptosis in trauma patients after high-energy lower extremity intra-articular fractures. *J. Orthopaedics Traumato.* **16**, 335–341 (2015).
62. J. A. Buckwalter *et al.*, The roles of mechanical stresses in the pathogenesis of osteoarthritis: Implications for treatment of joint injuries. *Cartilage* **4**, 286–294 (2013).
63. M. L. Delco *et al.*, Mitochondrial dysfunction is an acute response of articular chondrocytes to mechanical injury. *J. Orthopaedic Res®.* **36**, 739–750 (2018).
64. W. Lee *et al.*, Inflammatory signaling sensitizes Piezo1 mechanotransduction in articular chondrocytes as a pathogenic feed-forward mechanism in osteoarthritis. *Proc. Natl. Acad. Sci. U.S.A.* **118**, e2001611118 (2021).
65. S. Pritchard, F. Guilak, Effects of interleukin-1 on calcium signaling and the increase of filamentous actin in isolated and in situ articular chondrocytes. *Arthritis Rheumatism Off. J. Am. College Rheumatol.* **54**, 2164–2174 (2006).
66. S. Pritchard *et al.*, Interleukin-1 inhibits osmotically induced calcium signaling and volume regulation in articular chondrocytes. *Osteoarthritis Cartilage* **16**, 1466–1473 (2008).
67. C. Bae, F. Sachs, P. A. Gottlieb, The mechanosensitive ion channel Piezo1 is inhibited by the peptide GsMTx4. *Biochemistry* **50**, 6295–6300 (2011).
68. J. Guo *et al.*, Trends in piezo channel research over the past decade: A bibliometric analysis. *Front. Pharmacol.* **12**, 668714 (2021).
69. G. Haliloglu *et al.*, Recessive PIEZO2 stop mutation causes distal arthrogryposis with distal muscle weakness, scoliosis and proprioception defects. *J. Hum. Genet.* **62**, 497–501 (2017).
70. L. John *et al.*, The Piezo1 cation channel mediates uterine artery shear stress mechanotransduction and vasodilation during rat pregnancy. *Am. J. Physiol. Heart Circ. Physiol.* **315**, H1019–H1026 (2018).
71. T. M. Suchyna, *Piezo channels and GsMTx4:* Two milestones in our understanding of excitatory mechanosensitive channels and their role in pathology. *Progress Biophys. Mol. Biol.* **130**, 244–253 (2017).
72. H.-P. Lee, R. Stowers, O. Chaudhuri, Volume expansion and TRPV4 activation regulate stem cell fate in three-dimensional microenvironments. *Nat. Commun.* **10**, 529 (2019).
73. A. Liu *et al.*, Tunable fast relaxation in imine-based nanofibrillar hydrogels stimulates cell response through TRPV4 activation. *Biomacromolecules* **21**, 3745–3755 (2020).